

Fully Automated Region Growing Segmentation of Brain Lesion in Diffusion-weighted MRI

N. Mohd Saad, S.A.R. Abu-Bakar, Sobri Muda, M. Mokji, A.R. Abdullah

Abstract— This paper presents a fully automatic segmentation of brain lesions from diffusion-weighted magnetic resonance imaging (DW-MRI or DWI). The lesions are infarction, hemorrhage, tumor and abscess. Pre-processing stage is performed for intensity normalization, background removal and intensity enhancement. Then, split and merge algorithm is designed. Several statistical features are discussed and evaluated to select the best feature as homogeneity criteria. Lesions are segmented by merging the homogenous regions according to the selected criteria. This process produces blocky lesion region. Then, histogram thresholding is acquired to automate the seeds selection for region growing process. The region is iteratively grown by comparing all unallocated neighboring pixels to the seeds. The difference between pixel's intensity value and the region's mean is used as the similarity measure. The proposed segmentation technique has been validated by using misclassified area (MA), false positive rate (FPR), false negative rate (FNR), mean absolute percentage error (MAPE) and pixel absolute error ratio (r_{err}), and compared with previous methods. The result shows that automatic region growing method can successfully segment the lesions and is suitable for analysis and classification of DWI.

Index Terms— Diffusion-weighted MRI, brain lesion, segmentation, split and merge, region growing

I. INTRODUCTION

Tumor, infarction (stroke/ischemia), hemorrhage (bleeding/ ischemia) and infection (abscess) are the example of brain lesions that are affected in the brain cerebrum. In 2006, it was reported that tumor and brain diseases such as brain infarction and hemorrhage were the third and fourth leading cause of death in Malaysia [1]. The incidence of brain tumor in 2006 was 3.9 among males and 3.2 among females per 100,000 populations with a total of 664 cases reported by the Minister of Health Malaysia. In the United States, the combined incidence of primary brain tumor was 6.6 per 100,000 persons per year with a total of 22,070 new cases in 2009 [2], while brain infarction affects approximately 750,000 new cases per year [3].

Norhashimah Mohd Saad is with the Electronics and Computer Engineering department, Universiti Teknikal Malaysia Melaka, 76100, Durian Tunggal, Melaka, Malaysia (e-mail: norhashimah@utem.edu.my).

S. A. R. Abu-Bakar and M. Mokji are with the Computer, Vision, Video and Image Processing Research Lab, Faculty of Electrical Engineering, Universiti Teknologi Malaysia, 81310, Skudai, Johor, Malaysia (e-mail: syed@fke.utm.my, musa@fke.utm.my).

Sobri Muda is with Radiology Department, Medical Faculty, Universiti Kebangsaan Malaysia, Jalan Yaacob Latif, 56000 Cheras, Kuala Lumpur, Malaysia (e-mail: sobrimuda@yahoo.com).

A. R. Abdullah is with Electrical Engineering Department, Universiti Teknikal Malaysia Melaka, 76100, Durian Tunggal, Melaka, Malaysia (e-mail: abdulr@utem.edu.my).

Detection and diagnosis of brain lesion is the key for implementing successful therapy and treatment planning. However, the diagnosis is a very challenging task and can only be performed by professional neurologists. Any difficulty may necessitate more invasive examinations such as tissue biopsy [4]. Therefore, radiologists continuously seek for greater accuracy in the diagnosis of brain lesions from imaging investigations. Quantitative analysis may help radiologists to solve the problems. To assist visual interpretation of the medical images, computer-aided diagnosis (CAD) has become a major research subject in diagnostic radiology. With CAD, radiologists use the computer output as a second opinion in making the final decisions [5].

Diffusion-weighted magnetic resonance imaging (DW-MRI or DWI) has been widely used in the analysis of different medical conditions such as stroke, tumor and abscess. DWI measures the strength of water diffusion within a tissue structure, such as white matter (WM) and gray matter (GM), cerebral spinal fluid (CSF) and brain lesions (tumor, stroke, etc) which have their own particular diffusion character. Image contrast is depends on the diffusivity, where lesion or tissues with high diffusion appear dark (hypointense), and low diffusion appear bright (hyperintense) [6]. DWI provides higher lesion contrast compared to conventional MRI. It is considered as the most sensitive brain imaging in detecting acute stroke and hemorrhage [3, 7] and is useful in giving details of the lesion components [6, 8].

Accurate segmentation of DWI is desirable to allow interpretation of brain lesion structures in DWI. This process is performed visually by trained neurologists with a significant degree of precision and accuracy. Accurate segmentation is still a challenging task because of the variety of the possible shapes, locations and image intensities of various types of problems and protocols. For example, brain tumor segmentations in conventional MRI performed by experts have approximately 14–22% differences [9]. This process is time consuming and very subjective to make some treatment decisions [10].

Generally, the segmentation problem is very challenging and has yet to be solved. A large number of approaches have been proposed by various researchers to deal with MRI protocols. Well known and widely used segmentation techniques are k-means clustering algorithm, Fuzzy c-means (FCM) algorithm, Gaussian mixture model using Expectation Maximization (EM) algorithm, statistical classification using Gaussian Hidden Markov Random Field Model (GHMRF) and supervised method based on neural network classifier [11]. The commonly used segmentation techniques can be classified into two-broad categories: (1) region-based techniques that look for the regions satisfying

a given homogeneity criteria and (2) edge-based segmentation techniques that look for edges between regions with different characteristics [12]. For the region-based segmentation category, adaptive thresholding, clustering, region growing, watershed and split and merge are the well known methods for segmentation [13].

Region growing is one of the most popular techniques for segmentation of medical images due to its simplicity and good performance. The technique groups pixels or regions that have similar properties based on predefined criteria. It starts with a set of initial seed points that represent the criteria, and grow the region. Seeds can be automatically or manually selected [14]. Their automated selection can be based on finding pixels that are of interest. For example, the highest pixel from image histogram can serve as a seed pixel. On the other hand, seeds can also be selected manually from an image.

The focus of this study is to develop an automatic region growing algorithm that can accurately segment brain lesions in DWI. Pre-processing is first applied to the DWI for normalization, background removal and enhancement. Region splitting and merging is applied to produce blocky segmented region before region growing process is started. Simple statistical features based on histogram, mean of region and number of region pixels are used as homogeneity criteria to produce the segmentation. Segmentation efficiency is evaluated by comparing the results using clinical DWI dataset.

This paper is organized as follows. In section II, brain lesions characteristics in DWI are discussed in detail. Chapter III discussed the proposed research methodology. The flowchart of the segmentation process is detailed. As a pre-requisite, the theory behind the segmentation process is presented. The detail implementation of the proposed algorithms is also described in this chapter. Performance assessment metrics is discussed in Section IV. The segmentation results are shown and validated in Section V. Performance comparison with previous approach is also measured. In section VI, conclusions of this research work is presented.

II. DIFFUSION-WEIGHTED MRI

A. Brain Lesions

DWI has proven to be useful for evaluation of many brain lesions. It has proven valuable in distinguishing brain abscess from necrosis tumor, as these two lesions can have intensity overlap and difficult to differentiate in conventional MRI [15]. In acute infarction, changes in DWI may be revealed as early as 2 minutes after onset, whereas for conventional MRI and CT scan have sensitivities below 50% to detect of infarcts within 6 hours [16]. Fig.1 shows DWI intensities in major brain lesions, where the lesion is indicated by a white circle. In normal brain, the region consists of brain tissue and a cavity which is full of cerebral spinal fluid (CSF) located in the middle of the brain, as shown in Fig. 1(a). The DWI intensity for CSF is dark. Fig. 1 (b-f) shows several brain lesions, in which the intensity can be divided into hyperintense and hypointense. DWI hyperintense includes acute infarction, hemorrhage, solid tumor and abscess. Chronic infarction, hemorrhage and necrosis tumor appear hypointense.

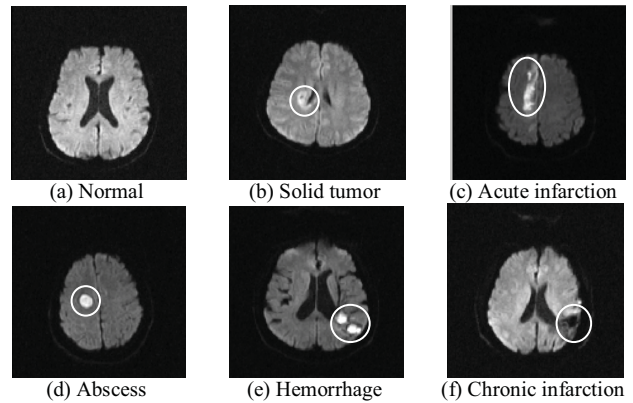


Fig. 1 Original DWI with brain lesion indicated by a white circle

TABLE I
DESCRIPTION OF BRAIN LESIONS, TYPES, SYMPTOMS AND PATHOLOGICAL FINDINGS [17-20]

Brain Lesion	DWI Characteristics	Symptoms	Pathological Findings
Tumor	Solid: Hyperintense Cystic/Necrosis: Hypointense	headache; Loss of balance; walking, visual and hearing problems; nausea; vomiting; unusual sleep; seizure	Abnormal growth of cells in uncontrolled manner shape: round, ellipse or irregular texture: clear, partially clear, blur
Infarction (Ischemia)	Acute / Subacute Hyperintense Chronic Hypointense	Paralysis; visual disturbances; speech problems; gait difficulties; altered level of consciousness	Cerebral vascular occlusion/ blockage
Hemorrhage (Bleeding)	Oxygenated hemoglobin / Acute hemorrhage Hyperintense Deoxy-hemoglobin / Chronic Hypointense	Paralysis; unconsciousness; visual disturbances; speech problems	Presence of blood products outside of the cerebral vascular
Abscess (Infection)	Hyperintense	Fever; seizure; headache; nausea; vomiting; altered mental status	Bacterial, viral or fungal infections, inflammatory and pus

The summary of major brain lesions, types, symptoms and pathological findings is summarized in Table I. High-grade solid tumors (glioma, lymphoma and metastasis; benign and malignant) typically are variable hyperintense on DWI. The common signal intensity of cystic tumor is hypointense. The tumors shape is commonly round, ellipse or heterogeneous lesion with mild or blur texture. Brain abscess is a lesion with inflammatory and pus due to bacterial or viral infection. Central small abscess may be seen as high signal on DWI.

Infarction (stroke) is classified as acute (less than 2 weeks) and chronic (3 weeks to 3 months), each having its characteristic abnormalities as shown in the table. Infarction is brain tissue damage due to vascular occlusion or blockage. Hemorrhage represents bleeding outside of the cerebral vascular. In the early stage of acute hemorrhage, the oxygenated blood product will be seen as hyperintense due to the high concentration of blood product. The DWI demonstrates hypointense on chronic hemorrhage created by deoxygenated blood product [16].

B. Imaging Protocol

The DW images have been acquired from the General Hospital of Kuala Lumpur using 1.5T MRI scanners Siemens Magnetom Avanto. Acquisition parameters used were time echo (TE), 94 ms; time repetition (TR), 3200 ms; pixel resolutions, 256 x 256; slice thickness, 5 mm; gap between each slice, 6.5 mm; intensity of diffusion weighting known as b value, 1000 s/mm² and total number of slices, 19. All samples have medical records which have been confirmed by at least 2 neurologists. Images were encoded in 12-bit DICOM (Digital Imaging and Communications in Medicine) format. The testing dataset consists of 3 abscess, 4 hemorrhage, 11 acute infarction, and 2 tumor which represent hyperintense lesions, and 3 samples for hypointense cases. In total, 20 hyperintense and 23 normal slices are used for validating the segmentation performance.

III. RESEARCH METHODOLOGY

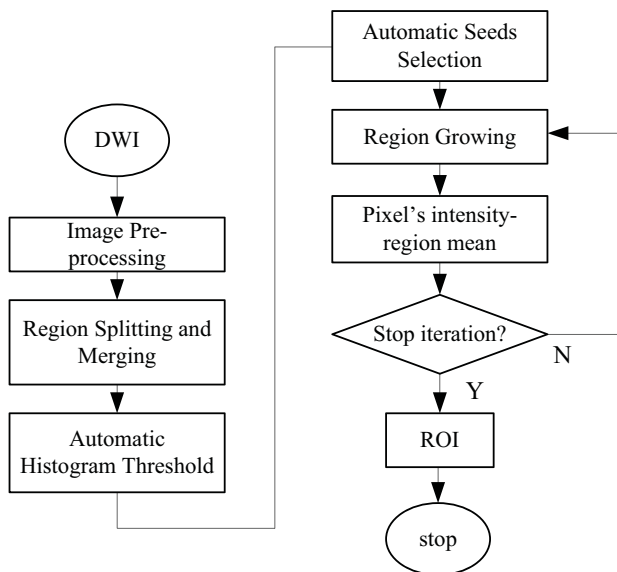


Fig. 2 Flowchart of the Segmentation Process

The flowchart of the whole analysis is shown in Fig. 2. The image is firstly pre-processed to normalize, remove the background and enhance the image intensity. Region splitting and merging is performed for region detection. Histogram is then calculated and an optimal threshold is acquired. Seed pixels are automatically selected from the pixels that are higher than the set optimal threshold value. After that, region growing is performed. The region is iteratively grown by comparing all unallocated neighboring pixels to the region. The difference between the pixel's

intensity value and the region's mean is used as a measure of similarity. This process stops when the intensity difference become larger than the difference between region's mean and optimal threshold.

A. Pre-processing Stage

Several pre-processing algorithms are applied to DWI for intensity normalization, background removal and intensity enhancement. The original DWI has 12-bit intensity depth unsigned integer. In normalization process, the type of the intensity depth is converted to double precision, where the minimum value is set to 0 while for the maximum is to 1. This process is required to simplify algorithm computation.

The DWI includes background image which needs to be removed. This is because the background shares similar gray level values with certain brain structures. This is done simply by using thresholding method [21]. From our experiments, the best threshold value has been set to 0.023. Then, the outer brain boundary is traced and the inner boundary is removed. Here, pixels that are inside the brain boundary are assigned as 1 (white) while the rest are set to 0 as background, as shown in Fig. 3(a). By multiplying this binary image to the original image, the brain image is obtained with background value equals to zero, as shown in Fig. 3(b). The steps of background removal can be summarized as follows:

1. Convert the image into binary using thresholding method.
2. Trace the outer region boundaries based on edge.
3. Run morphological operation to remove small pixels.

Next, Gamma-law transformation algorithm is chosen to enhance the narrow range of low input gray level values of the DWI to a wider range. It has the basic form of $s = cr^\gamma$, where s is the output gray level intensity, c is the amplitude, and γ is the constant power of the input gray level, r [22]. $\gamma=0.4$ has been found to be the best value based on experiments to enhance the output histogram. Plot of s versus r for $\gamma=0.4$ is shown in Fig. 4. Typically, Gamma-law curves with values of $\gamma < 1$ expand the gray level intensity of dark area in input, r , and produce enhanced output, s .

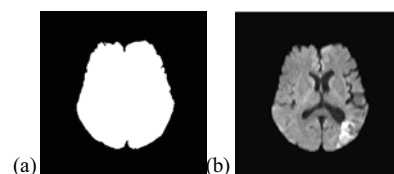


Fig. 3 DWI at pre-processing stage: (a) image after thresholding and boundary tracing (b) image after background removal

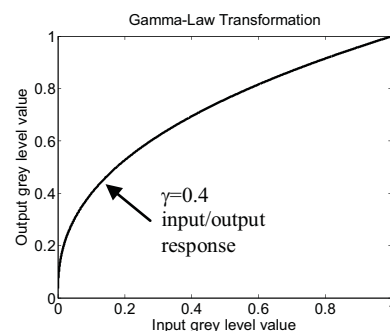


Fig. 4 Gamma-law response with constant power of $\gamma=0.4$

Fig. 5 illustrates the results of preprocessing steps. Fig. 5(a) shows the original normalized image and its histogram. In Fig. 5(b), all background pixels have been removed, and therefore improve the shape of the image histogram which strongly bimodal between CSF and tissue components. The maximum peak is located at 0.1. The intensity range for the background removed image lies between 0 and 0.15, which is very dark and narrow. After applying Gamma-law transformation algorithm, the histogram has been enhanced in which the peak is located at 0.4 as shown in Fig. 5(c).

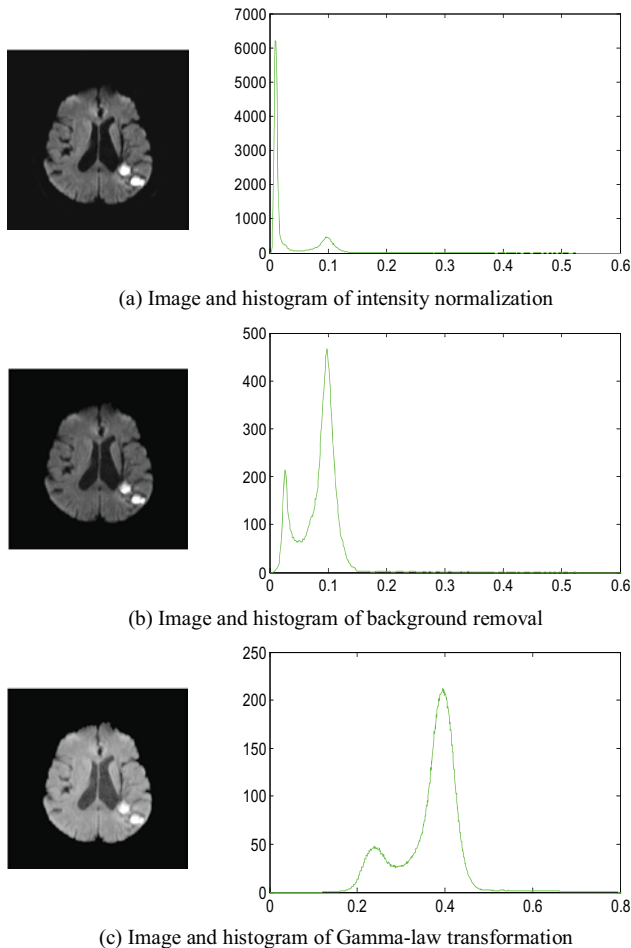


Fig. 5: Pre-processing steps for segmentation. (a) Original normalized image, (b) Result of background removal, (c) Result of Gamma-law transformation. Corresponding histogram are shown on the right.

B. Split and Merge Algorithm

Split and merge algorithm [23, 24] is based on a quad tree structure representation whereby a square image segment is broken (split) into four quadrants if the original image is non-uniform in attribute. If four neighboring squares are found to be uniform, they are replaced (merged) by a single square composed of the four adjacent squares.

Fig. 6 shows the representation of the quad tree structure. The process is divided into three partition levels. Each level splits the region into four sub-regions. Statistical features are calculated to find the homogeneity criteria. The regions that are homogenous to the criteria are then merged to form the ROI.

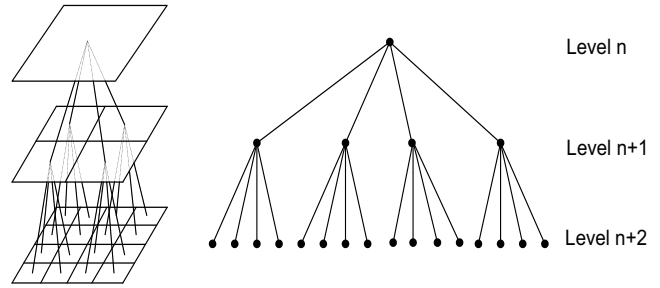


Fig. 6 The quad tree structure [25]

Fig. 7 shows the process in DWI, which is outlined by specific line weights. The splitting levels divided the image into another four sub-regions. The first partition level is outlined by thick cross-lines, the second and the third levels are specified by light weight white colors. The merged level is outlined by a thick box. It is the final segmentation result that forms the ROI.

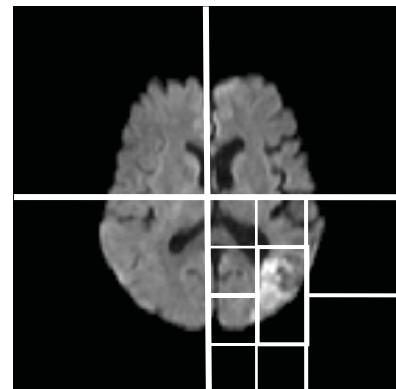


Fig. 7 Example of the split and merge segmentation process. The thick box shows the merged segmentation region

C. Homogeneity Criteria

First order statistics are used to represent intensity of level of the image. The statistical features that are frequently used are mean and standard deviation. Mean is average value of a random variable. Standard deviation is the variation from its mean. Let i be the random variable representing the N intensity levels of the image and $P(i)$ is its histogram, its mean and standard deviation can be defined by Eq. (1) and Eq. (2) [26] respectively.

$$\mu = \frac{1}{N} \sum_{i=1}^{N-1} P(i) \quad (1)$$

$$\sigma = \sqrt{\frac{1}{N} \sum_{i=0}^{N-1} (P(i) - \mu)^2} \quad (2)$$

Another parameter that results from histogram is entropy. It measures histogram uniformity, in which the closer the histogram is to the uniform distribution, the higher is the entropy [26]. Entropy can be defined by

$$Entr = - \sum_{i=0}^{N-1} P(i) \log_2 P(i) \quad (3)$$

Fig. 8 shows region 3 and region 4 at first partition level. In this figure, there is a hyperintense lesion in region 4, while region 3 appears normal. Their histogram distribution is shown in Fig. 9. The intensity range of the lesion can be acquired from the histogram and the optimal threshold is determined based on the average value obtained from dataset.

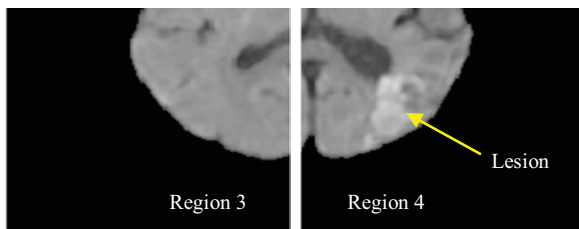


Fig. 8 Region splitting at first stage shows split image of region 3 and 4, the arrow in region 4 shows hyperintense lesion

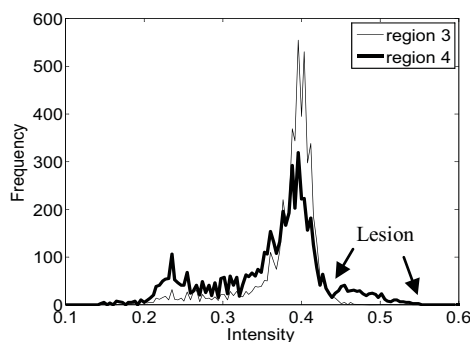


Fig. 9 Histogram of region 3 and 4, the arrow shows the histogram of hyperintense lesion

Table II shows the optimal threshold value based on histogram. The minimum and maximum hyperintense is 0.47 and 0.8, respectively, whilst for hypointense the value is 0.1 and 0.25.

TABLE II
INTENSITY OF LESIONS BASED ON HISTOGRAM

Optimal Threshold of Lesion Appearance			
Hyperintense		Hypointense	
Minimum	Maximum	Minimum	Maximum
0.47	0.8	0.1	0.25

Table III shows the setting value of homogeneity criteria for hyperintense and hypointense lesions. The homogeneity criteria calculated within the lesion are mean and number of lesion pixels. Mean of lesion is chosen because it is the most uniform criterion for lesion detection. Mean value for hyperintense is high because the intensity is bright, whilst for hypointense, the value is low. The mean for hyperintense and hypointense has been set to 0.495 and 0.2, respectively. Both values are chosen based on average from the samples.

TABLE III
THRESHOLD VALUE OF SELECTED HOMOGENEITY CRITERIA

Type of Lesion	Selected Homogeneity Criteria	
	Minimum Mean of Lesion, μ	Minimum Number of Lesion Pixels, N
Hyperintense Lesion	$\mu > 0.495$	$N > 30$
Hypointense Lesion	$\mu \leq 0.2$ and $\mu \neq 0$	$N > 100$

For hypointense, the mean must not equal to zero since it is the background value. If the mean is smaller than its set, then the number of lesion pixels is used. From our dataset, the smallest number of pixels for hyperintense and hypointense is 30 and 100, respectively. The region is selected for the next level if the number of lesion pixels is higher than these values.

Fig. 10 shows region 4 from the first partition level is further split to four regions at the second partition level. This figure shows the regions with lesion appearance at region 4-1 and region 4-3.

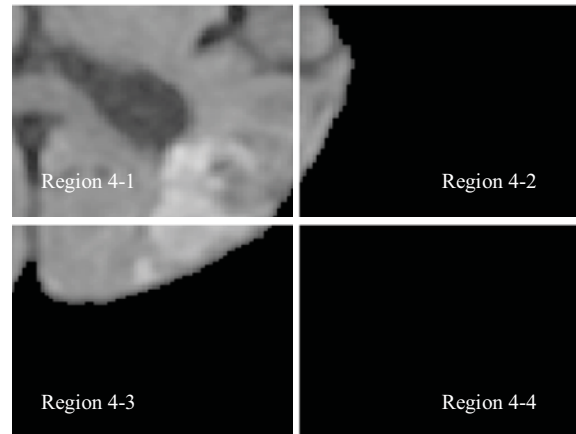


Fig. 10 Region splitting at second level with lesion appearance in region 4-1 and 4-3

Statistical features in the area of lesion are shown in Table IV. The features are standard deviation, entropy, mean and number of lesion pixels. From the table, the statistical values for region 4-2 and region 4-4 are zero because there is no lesion pixel. For region 4-1 and region 4-3, the number of lesion pixels is 216 and 47, respectively. The mean of lesion for both regions are 0.4977 and 0.4824.

The mean for region 4-1 is higher than its set and is selected for the next partition level. For region 4-3, the mean is smaller than its set. However, its number of lesion pixels is higher than 30, thus this region is also selected for the next partition level. Standard deviation and entropy are also calculated for all levels. From this table, standard deviation is low since all pixels intensities of the lesion are closer to its mean. For the entropy, the value for region 4-1 is higher because it depends on the total number of lesion pixels, whilst for region 4-3 the value is lower. Thereby both standard deviation and entropy are not selected as homogeneity criteria.

TABLE IV
STATISTICAL FEATURES FOR LESIONS IN REGION SPLITTING LEVEL 2

Region	Pixel Size	Statistical Features in area of Lesion			
		Standard Deviation of Lesion, σ	Entropy of Lesion, $Entr$	Mean of Lesion, μ	Number of Lesion Pixels, N
4-1	64x64	0.0194821	5.7067	0.497655	216
4-2		0	0	0	0
4-3		0.008541	4.2932	0.482429	47
4-4		0	0	0	0

The process of splitting is then continued to the third partition level. This is the final level, in which each block, size is 32x32. Fig. 11 shows the example of the third partition level for region 4-1.

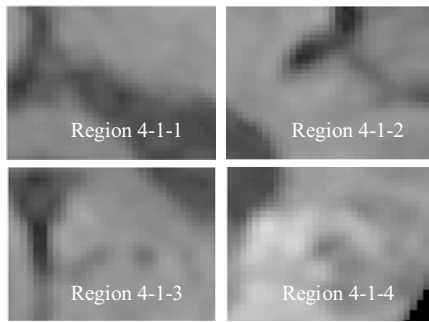


Fig. 11 Region splitting at third level with lesion appearance in 4-1-4

From the split regions, their statistical features are again calculated, as shown in Table V. From the table, only region 4-1-4 has lesion appearance. The mean is 0.4977 and the number of lesion pixels is 216 which are similar to the values in the second partition level, region 4-1. Thus, only this region is selected for segmentation. Similar process is also calculated for region 4-3 to calculate the third partition level. Lesion regions are then merged to get the final segmentation result.

TABLE V
STATISTICAL FEATURES FOR LESIONS IN REGION SPLITTING LEVEL 3

Region	Pixel Size	Statistical Features in area of Lesion			
		Standard Deviation of Lesion, σ	Entropy of Lesion, $Entr$	Mean of Lesion, μ	Number of Lesion Pixels, N
4-1-1	32x32	0	0	0	0
4-1-2		0	0	0	0
4-1-3		0	0	0	0
4-1-4		0.019482 1	5.7067	0.49765 5	216

D. Region Growing Segmentation Process

Region growing is a procedure that groups pixels or sub regions into larger regions based on predefined criteria. Seeded region growing requires seeds as additional input. The basic approach is to start with a set of seed points and grow the regions by appending to each seed's neighboring pixels that have similar properties to the seed. The region growing algorithm applied in this study is summarized as follows:

1. Histogram: calculate histogram of the merged segmentation region.
2. Automatic thresholding: calculate divergence measure using Eq. (4), where $P(i)$ is histogram from step 1.

$$div(i) = \frac{dy}{dx} P(i) \quad (4)$$

3. Set optimal threshold at the first nearest to zero value after divergence's maximum peak.

4. Automatic Seeds selection: Select pixels that are higher than the optimal threshold as seeds.
 5. Region Growing: select the 1st seed pixel as the first region mean. Grow the region by comparing with neighboring pixels to this region.
 6. Measure the difference between the pixel's intensity with the region's mean. The growing process is stopped when this intensity difference is larger than the difference between region's mean and optimal threshold, shows in Eq. (5) and (6).
- $$I(x,y) - \mu \geq T \quad (5)$$
- $$T = \mu - T_{optimal} \quad (6)$$
7. Repeat step 4 to 6 until there are no more seed pixel that does not belong to any segmented region.

Fig. 12 illustrates the DWI of acute infarction. Fig. 12 (a) shows the pre-processed image and the results after the splitting and merging process. As for automatic seeds selection, histogram from the lesion region is calculated (shown in Fig. 13(a)). Optimal threshold value is acquired by measuring the divergence from the histogram. The divergence reaches its maximum when the histogram is at the greatest rate of change. The optimal threshold is set at the first nearest to zero divergence value after the maximum peak. Each pixel higher than this value is assigned as seeds. The divergence is shown in Fig. 13 (b).

Once the seed point is selected, the region growing process is started. When the growth of one region stops, it will choose another seed pixel which does not yet belong to any segmented region and the process will start again. The iterations stop when all seeds have been used for the region growth.

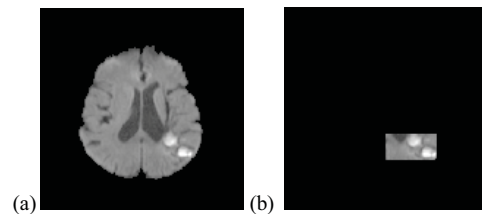


Fig. 12 (a) Acute infarction image (b) Image after region splitting and merging

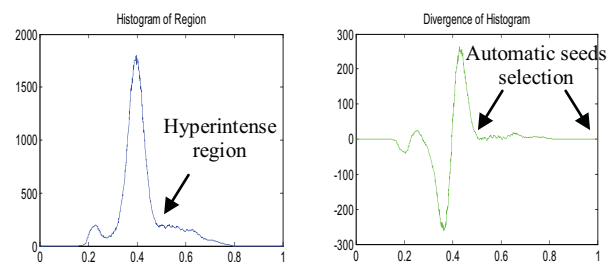


Fig. 13 (a) Histogram of region (b) Divergence measure from histogram

IV. PERFORMANCE ASSESSMENT METRICS

Performance assessment of the segmentation results is done by comparing the ROI results obtained from the analysis with the manual segmentation which has been visually inspected by neurologist. Area overlap (AO), false positive rate (FPR), false negative rate (FNR) and

misclassified area (MA) are used as the performance metrics. These metrics are computed as follows [27]

$$AO = 100 \times \frac{S_1 \cap S_2^c}{S_1 \cup S_2} \quad (7)$$

$$FPR = 100 \times \frac{S_1 \cap S_2^c}{S_1 \cup S_2} \quad (8)$$

$$FNR = 100 \times \frac{S_1^c \cap S_2}{S_1 \cup S_2} \quad (9)$$

$$\begin{aligned} MA &= 1 - AO \\ &= FPR + FNR \end{aligned} \quad (10)$$

where S_1 represents the segmentation results obtained by the algorithm and S_2 represents the manual segmentation. AO computes the segmented similarity by comparing the overlap region between the manual and the automatic segmentation. FPR and FNR are used to quantify over-segmentation and under-segmentation respectively. High AO, and low FPR and FNR showed low error, i.e. high accuracy of the measurement. MA must be low to provide better segmentation accuracy.

Mean absolute percentage error (MAPE) was used as index for misclassified index for mean and number of pixels value in the segmentation area, while pixel absolute error ratio (r_{err}) was for misclassified pixels for normal control. MAPE is an index that measures the difference between actual and measured value and is expressed as

$$MAPE = 100 \times \frac{|S_1 - S_2|}{S_1} \quad (11)$$

Besides MAPE, absolute error ratio, r_{err} is also applied to quantify the accuracy of the segmentation for normal image. r_{err} is defined as the ratio between the absolute difference in the number of over segmented pixels between the actual and the proposed segmentation method, n_{diff} , and the total number of pixels, N , of an image. Normal image should result in 0 number of pixel in the segmented image. Otherwise the result is over segmented.

$$r_{err} = \frac{n_{diff}}{N} \times 100\% \quad (12)$$

Low MA, MAPE and r_{err} show low error, which is high similarity with respect to neurologist's judgments.

V. RESULTS

The proposed method has been tested on our dataset, as discussed in section II. Fig. 14 shows six samples of hyperintense lesion, indicated by white circle and their segmentation results. The lesions are indicated by white circle. Fig. 14 (a-d) show DWI with acute infarction and

their segmentation results are shown on the second row of each image. Fig. 14 (e-f) show tumor and abscess, and their segmentation results are shown on the next row. The figures show that the proposed method has successfully segmented the hyperintense lesion, even in very small acute infarction in Fig. 14(c).

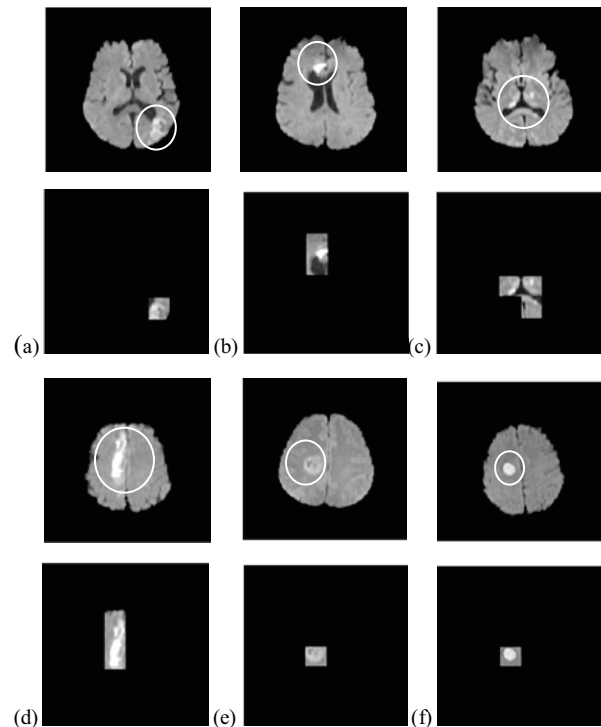


Fig. 14 Hyperintense lesions and split and merge segmentation results: (a-d) acute infarction, (e) tumor, (f) abscess

Fig. 15 shows hypointense lesion and normal samples and their segmentation results. Fig. 15 (a-b) show DW images with chronic infarction and their segmentation results are shown on the second row. For normal brain, no region is segmented. The normal brain has a cavity which is full of cerebral spinal fluid (CSF) at the centre of the brain. The intensity is dark, which is similar to the intensity of the hypointense lesion and normally symmetric, as shown in Fig. 15(c). To remove the CSF from being segmented with the hypointense lesion, detection based on location is used. It is simply done by removing the CSF regions at the merge level. The regions are 1-4-4, 2-3-3, 3-2-2, 4-1-1, 3-2-4, and 4-1-3.

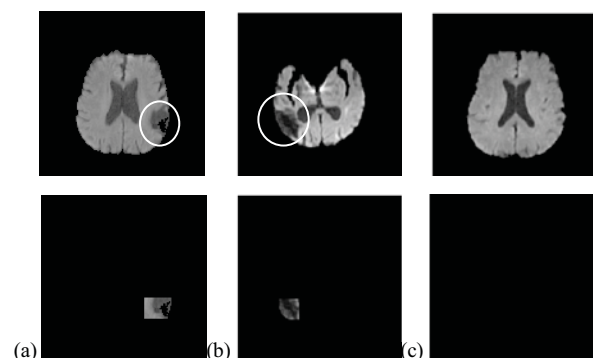


Fig. 15 Split and Merge Segmentation Results for hypointense lesion and normal

Fig. 16 shows the final results of hyperintense segmentation, while Fig 17 shows the hypointense segmentation. The figures clearly show that the proposed segmentation algorithms can successfully segment the lesions.

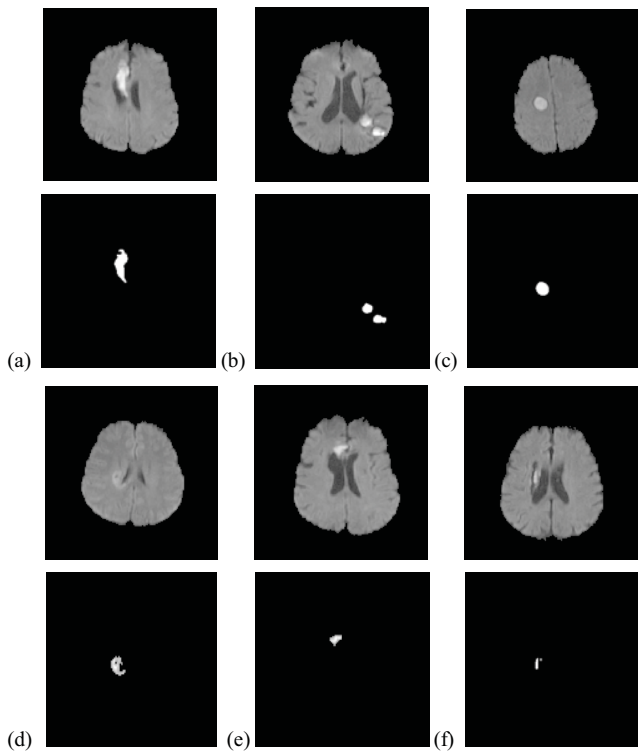


Fig. 16 Hyperintense lesions and their segmentation results: (a) acute infarction, (b) hemorrhage, (c) abscess, (d) tumor, (e) acute infarction, (f) hemorrhage

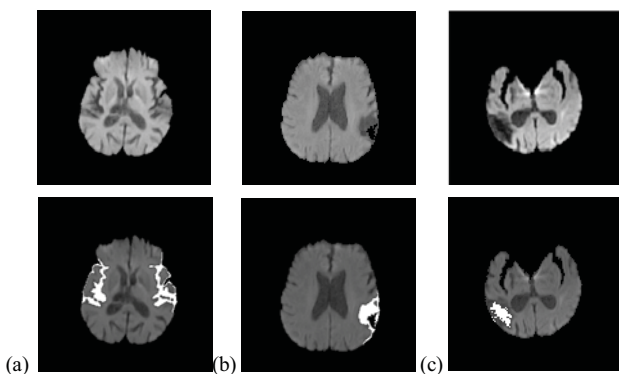


Fig. 17 Hypointense lesions and their segmentation results: (a) - (c) chronic stroke

Fig. 18 shows average segmentation performance of the proposed automatic region growing method with comparison of semi-automatic region growing [28]. Semi-automatic region growing provides lower misclassified area (MA) which means better similarity to manual segmentation. This is expected because semi-automatic segmentation is usually applied if automatic segmentation is not accurate enough.

In this analysis, MA of the automatic algorithms is comparable with the semi-automatic. Both segmentations provide almost similar performance. On the other hand, the automatic segmentation provides better mean absolute percentage error (MAPE) compared to the manual segmentation results. For normal control, the misclassified

pixel (r_{err}) is very small. This measurement is not applicable for semi-automatic segmentation. Overall, the automatic region growing provides comparable results with the semi-automatic segmentation technique.

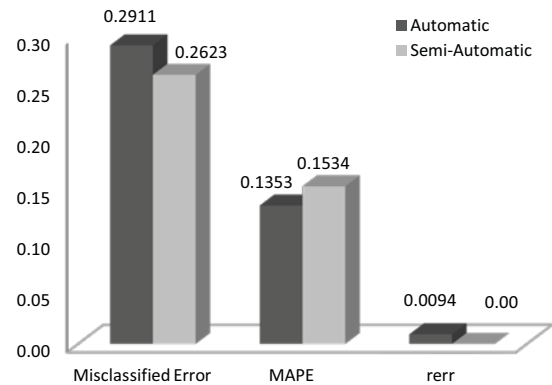


Fig. 18 Average performance of the algorithm

Table VI shows the performance evaluation between the proposed fully automatic segmentation, with comparison of conventional semi-automatic region growing. The results show that the proposed automatic method offers very good segmentation results for abscess, hemorrhage and infarction. It provides comparable performance with semi-automatic segmentation. However, it has a slightly remarkable difference for tumor. The automatic segmentation cannot fully characterize the tumor lesion as good as semi-automatic region growing. In addition, some tumor lesions consist of fuzzy boundary and iso-intense area compared to the other type of lesions. The errors for under-segmentation (FNR) are bigger than over-segmentation (FPR) for all cases. The shaded areas show the best average performance.

TABLE VI
PERFORMANCE EVALUATION FOR EACH LESIONS: COMPARISON BETWEEN THE PROPOSED AUTOMATIC REGION GROWING WITH SEMI-AUTOMATIC REGION GROWING TECHNIQUES

Index	Area Overlap		False Positive Rate (over-segmentation)		False Negative Rate (under-segmentation)	
	Auto R. Growin g	Semi-auto R. Growing	Auto R. Growing	Semi-auto R. Growing	Auto R. Growing	Semi-auto R. Growing
Abscess	0.2504	0.2158	0.0161	0.0056	0.2343	0.2102
Hemorrhage	0.2980	0.3029	0.0850	0.0395	0.2130	0.2634
Infarction	0.2755	0.2249	0.0837	0.0211	0.1918	0.2038
Tumor	0.3458	0.1841	0.1072	0.1001	0.2386	0.0840
Average	0.2911	0.2623	0.0766	0.0368	0.2145	0.2255

Fig. 19 shows comparison of segmentation performance of the proposed automatic region growing method and semi-automatic region growing with gray level co-occurrence matrix (GLCM) and thresholding techniques. For reference, GCLM and thresholding techniques have been discussed in [29]. As described in the subchapter VI, low misclassified error, over segmentation and under segmentation errors (FPR and FNR), mean absolute percentage error (MAPE) and misclassified pixels (r_{err}) show high accuracy of the measurements with respect to the neurologist's judgments.

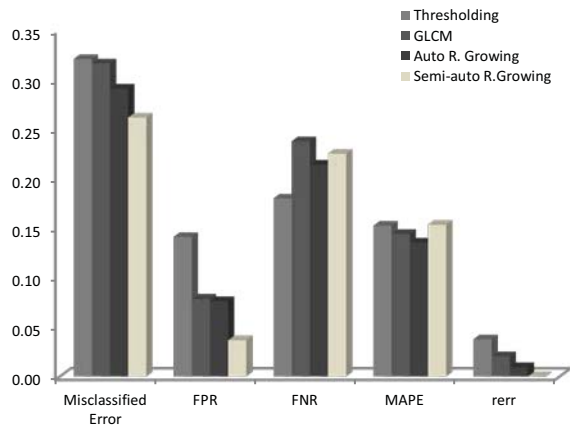


Fig. 19 Average performance of the algorithms comparison with thresholding and gray level co-occurrence matrix [29]

The comparison performance is detailed in Table VII. The shaded area in the table shows the highest accuracy. Both region growing methods provide lower misclassified error, FPR and FNR, MAPE and r_{err} compared to GLCM and thresholding techniques which means more accuracy. Overall, the automatic region growing provides better segmentation accuracy compared to GLCM and thresholding techniques.

TABLE VII

COMPARISON BETWEEN THRESHOLDING, GRAY LEVEL CO-OCCURRENCE MATRIX, AUTOMATIC REGION GROWING AND SEMI-AUTOMATIC REGION GROWING TECHNIQUES

	Misclassified Error	FPR	FNR	MAPE	r_{err}
Thresholding	0.3211	0.1410	0.1801	0.1524	0.0377
GLCM	0.3167	0.0785	0.2381	0.1440	0.0205
Auto Region Growing	0.2911	0.0766	0.2145	0.1353	0.0094
Semi automated Region Growing	0.2623	0.0368	0.2255	0.1534	0.0000

VI. CONCLUSION

This paper described segmentation of brain lesion in diffusion-weighted MRI (DWI) using automated region growing approach. It used clinical DWI lesions such as infarction, hemorrhage, tumor and abscess. Region splitting and merging was carried out to obtain the lesion region. Histogram thresholding was used to find the optimal intensity threshold value and to obtain automatic seeds selection. The regions according to hyperintense and hypointense lesions were segmented. Comparison with gray level co-occurrence matrix (GLCM) and thresholding techniques were also obtained. The results have shown that the automatic region growing provides comparable results with the semi-automatic region growing segmentation. The proposed method can successfully segment the lesions and suitable for analysis of DWI and for classification purpose. Overall, automatic region growing provides better segmentation accuracy compared to GLCM and thresholding techniques.

This work was supported by Universiti Teknikal Malaysia Melaka (UTeM), Universiti Teknologi Malaysia (UTM) and Ministry of Higher Education (MoHE) under Research University Grant Q.J13000.7123.00H53. We also thank Universiti Kebangsaan Malaysia Medical Centre (UKMMC) for collaborating in medical knowledge and providing dataset for this research work.

REFERENCES

- [1] Malaysian Cancer Statistics – Data and Figure Peninsular Malaysia 2006, National Cancer Registry, Ministry of Health, Malaysia.
- [2] American Cancer Society: Cancer Facts and Figures 2009. Atlanta, Ga: American Cancer Society, 2009.
- [3] Magnetom Maestro Class, “Diffusion weighted MRI of the brain” Brochure Siemens Medical Solutions that helps.
- [4] M. Barnathan, J. Zhang, E. Miranda, V. Megalooikonomou, “A texture-based for identifying tissue type in magnetic resonance images” *IEEE International Symposium on Biomedical Imaging (ISBI): from Nano to Macro*, pp.464-467, 2008.
- [5] K. Doi, “Computer-aided diagnosis in medical imaging: Historical review, current status and future potential” *Computerized Medical Imaging and Graphics*, vol.31, pp. 198–211, 2007.
- [6] P.W. Schaefer, P.E. Grant, R.G. Gonzalez, “State of the Art: Diffusion-weighted MR imaging of the brain.” *Annual Meetings of the Radiological Society of North America (RSNA)*, 2000.
- [7] S.J. Holdsworth, R. Bammer, “Magnetic resonance imaging techniques: fMRI, DWI, and PWI.” *Seminars in Neurology*, Vol.28, Number 4, 2008.
- [8] S.K. Mukherji, T.L. Chenevert, M. Castillo, “State of the Art: Diffusion-Weighted Magnetic Resonance Imaging.” *Journal of Neuro-Ophthalmology*, Vol.22, No.2, 2002.
- [9] I. Guler, A. Demirhan, R. Karakis, “Interpretation of MR images using self-organizing maps and knowledge based expert systems” *Elsevier J. Digital Signal Processing*, vol.19, pp.668-677, 2009.
- [10] W. L. Nowinski, G. Qian, K.N. Bhanu Prakash, I. Volkau, et al. “Stroke Cad: Cad Systems for Acute Ischemic Stroke, Hemorrhagic Stroke, and Stroke in ER” *MIMI 2007, LNCS 4987*, pp.277-386, 2008.
- [11] Rubens Cardenes, Rodrigo de Luis-Garcia, Meritxell Bach-Cuadra, “A multidimensional segmentation evaluation for medical image data” *J. Computer Methods and Programs in Medicine*, vol.96, pp.108-124, 2009.
- [12] I.N. Bankman, “Handbook of medical imaging: processing and analysis eleventh edition” Academic Press, 2000.
- [13] William K. Pratt, “Digital Image Processing, 3rd Edition” John Wiley & Sons Inc., 2001.
- [14] R. B. Dubey, M. Hanmandlu, S. K. Gupta, S. K. Gupta, “Region Growing for MRI brain tumor volume analysis” *Indian Journal of Science and Technology*, Vol.2 No. 9, 2009, pp.26-31.
- [15] Ping H.L., Jih T.H., Wei L.C., et al. “Brain Abscess and Necrotic Brain Tumor: Discrimination with Proton MR Spectroscopy and Diffusion-Weighted Imaging” *AJNR Am J Neuroradiol* 23:1369–1377, September 2002.
- [16] T. Moritani, · S. Ekholm, · P.-L. Westesson, “Diffusion-Weighted MR Imaging of the Brain” ISBN-13 978-3-540-25359-4, Springer, 2005.
- [17] S. Cha, “Review Article: Update on Brain Tumor Imaging: From Anatomy to Physiology”, *Journal of Neuroradiology*, vol.27, pp.475-487, 2006.
- [18] M.D.Hammer, L.R.Wechsler, “Neuroimaging in ischemia and infarction.” *Seminars in Neurology* Vol.28, Number 4, 2008.
- [19] R.T.Ullrich, L.W.Kracht, A.H.Jacobs, “Neuroimaging in patients with gliomas.” *Seminars in Neurology* Vol.28, Number 4, 2008.
- [20] O. Kastrop, I. Wanke, M. Maschke, “Neuroimaging of infections of the central nervous system.” *Seminars in Neurology* Vol.28, Number 4, 2008.
- [21] Otsu, N., "A Threshold Selection Method from Gray-Level Histograms." *IEEE Transactions on Systems, Man, and Cybernetics*, Vol. 9, No. 1, 1979, pp. 62-66.
- [22] R.C. Gonzalez, R.E. Woods, “Digital Image Processing second edition.” Prentice Hall, 2001.
- [23] T. Pavlidis, “Algorithms for graphics and image processing” Computer Science Press, Rockville, MD, 1982.

- [24] S.L. Horowitz, T. Pavlidis, "Picture segmentation by a tree transversal algorithm" *J. Assoc. for Computing Machinery*, vol. 23, 1976, pp.368-388.
- [25] K.C. Straster, J.J. Gerbrands, "Three-dimensional image segmentation using a split, merge and group approach" *Pattern Recognition Letters*, Vol.12, 1991, pp.307-325.
- [26] J. Ramirez, J.M. Górriz, D. Salas-Gonzalez, "Computer-aided diagnosis of Alzheimer's type dementia combining support vector machines and discriminant set of features", *Elsevier J. Information Sciences*, 2009.
- [27] J.G. Park, C. Lee, "Skull Stripping based on region growing for magnetic resonance images", *J. NeuroImage*, vol.47, 2009, pp. 1394-1407.
- [28] N. Mohd Saad, S.A.R. Abu-Bakar, Sobri Muda, M. Mokji, A.R. Abdullah, "Automated Region Growing for Segmentation of Brain Lesion in Diffusion-weighted MRI", *Proceedings of The International MultiConference of Engineers and Computer Scientists 2012, IMECS 2012*, 14-16 March, 2012, Hong Kong, pp.674-677.
- [29] N. Mohd Saad, S.A.R. Abu-Bakar, A.R. Abdullah, L. Salahuddin, Sobri Muda, M. Mokji, "Brain Lesion Segmentation From Diffusion-Weighted MRI Based On Adaptive Thresholding And Gray Level Co-Occurrence Matrix", *J. Telecommunication Electronic and Computer Engineering*, Vol. 3 No. 2, 2011.